CrossMark

Thermo-structural analysis of TeO$_2$–Li$_2$O–MoO$_3$ glasses

João L. Gomes Jr[1] · Anderson Gonçalves[1] · Aloisi Somer[1] · Jaqueline V. Gunha[1] · Gerson K. Cruz[1] · Andressa Novatski[1]

Abstract

This work discusses some new insights into the structural and thermal properties of the glass system TeO$_2$–Li$_2$O–MoO$_3$. Glasses in the composition $(80 - 2x)$ TeO$_2$ − xLi$_2$O − $(20 + x)$ MoO$_3$ (TLM) where $x = 0, 5, 10, 15$ and 20 mol% were prepared by the melt-quenching technique and were characterized by X-ray diffraction (XRD), Raman spectroscopy, density, refractive index, and differential scanning calorimetry (DSC). XRD data confirmed the amorphous character of the samples. In addition, the glass transition (T_g), the onset crystallization (T_x), and the first exothermic peak at the crystallization temperatures (T_c) were determined from DSC scans. Thermal stability ($\Delta T = T_x - T_g$) increases up to $x = 15$ mol% followed by a decrease for higher x. Raman results showed that when x increases, the Te–O–Mo linkages form, meaning that Li$_2$O addition breaks the Te units and Mo-units in the studied glasses. The Te–O–Mo linkages enhance the thermal stability values, increasing the oxygen packing density. The formation of these linkages also alters the refractive index and the electronic polarizability behaviors. In summary, this work shows that the addition of Li$_2$O in the TeO$_2$–MoO$_3$ system enhances the thermal stability and changes the electronic polarizability behavior, showing the potential of the studied material for technological applications.

Keywords Tellurite glasses · Characteristic temperature · Density · Molar volume · Molecular electron polarizability

Introduction

Oxide glasses have been the subject of increasing interest for optical and electronic devices [17]. TeO$_2$-based glasses, for instance, are attractive for such applications due to the low melting temperature point ($T_m \backsim 973$ K) [2, 10, 14, 16, 44], high thermal stability ($\Delta T > 373$ K) [14, 16, 42, 46], high linear and nonlinear refractive indices ($n_0 \backsim 2.2$ and $\chi^3 \backsim 8.0 \times 10^{-13}$ esu, respectively) [10, 13, 21, 23, 27, 33, 44], wide optical transmission range (0.35–5 μm) [19, 49], high optical basicity, and electronic polarizability values [9, 10, 21, 42].

Unlike the classical forming oxides SiO$_2$ and GeO$_2$, TeO$_2$-pure glass is obtained only under controlled conditions. The addition of modifying oxides, such as Li$_2$O, promotes a reduction in the glass transition temperature (T_g), increasing the ΔT [37, 38, 48, 50]. This effect is associated with the breaking of Te–O bonds in TeO$_4$ units, creating TeO$_{3+1}$ and TeO$_3$ units. This variation of the coordination state of Te atom increases the non-bridging oxygen (NBO) content in glass network, changing thermal and optical properties [13]. Alternatively, adding transition metal oxides such as MoO$_3$, ZnO, Nb$_2$O$_5$ or Ag$_2$O improves on the thermal, optical, and semiconductive properties [22, 26, 30, 32, 36, 43, 44, 47].

Physico-chemical properties of binary telluride glass containing MoO$_3$ oxide are widely studied in mechanical engineering applications [49]. The structural properties of Te–Mo glasses have also been previously investigated using spectroscopic techniques [7, 34, 39] and X-ray photoelectron spectroscopy (XPS) [31]. These investigations proposed that MoO$_3$ can act as a former or a modifier network, and depending upon its role, the desired properties of TeO$_2$–MoO$_3$ glassy system change.

Adding multiple components into a glassy system in a controlled manner allows the extension of the functional applicability of these glasses [4]. Consequently, a detailed

✉ João L. Gomes Jr
gomesjr.jl@gmail.com

[1] Departamento de Física, Universidade Estadual de Ponta Grossa, Ponta Grossa, PR 84030-900, Brazil

investigation of the thermal and optical properties should be made regarding the function of the structural alteration in the function of composition. In this sense, this work investigates the structural and thermal properties of the ternary system $(80 - 2x)\,TeO_2 - x\,Li_2O - (20 + x)\,MoO_3$ (TLM) where $x = 0, 5, 10, 15$ and 20 mol%.

Materials and methods

Samples in the composition $(80 - 2x)TeO_2 - (20 + x)MoO_3$ (TLM) where $x = 0, 5, 10, 15$ and 20 mol% were prepared using the TeO_2 (Alfa Aesar 4N), Li_2CO_3 (LAFAN 3N), and MoO_3 (Vetec 2N) oxide powders.

The powders were mixed and macerated in an agate mortar for 50 min. For the melt-quenching method, the mixture was heated in a platinum crucible in a furnace and melted at the temperature of 1123 K. The quenching was done in a brass mold heated at 20 K below the T_g and followed by heat treatment at this temperature for 4 h.

X-ray diffraction measurements were performed using a Rigaku Ultima IV X-ray automatic diffractometer (Cu K_α radiation, $\lambda = 1.5418$ Å, 30 kV, 40 mA) at a scan rate of $2°\,min^{-1}$ to confirm the amorphous nature of samples. The Raman spectra were recorded by a Brüker spectrometer model Senterra, laser excitation at 532 nm, 20 mW, 1200 grooves/mm. The integration time was 20 s using a $20\times$ objective.

Thermal analyses were performed using a differential scanning calorimetry (DSC) Setaram Instrumentation model Labsys Evo. The heating rate was $10\,K\,min^{-1}$ in argon atmosphere (flow at $20\,mL\,min^{-1}$) from room temperature to 873 K in an alumina crucible. Density of the samples were determined using the Archimedes principle. Samples (in bulk) were submerged in distilled water at room temperature and constant pressure, and the measurements were performed using a balance Shimadzu AY220 with an accuracy of 10^{-4} g.

The linear refractive index (n_0) values were determined by the Brewster angle method [3, 23]. The light source was a laser He–Ne JDSU brand, model 1137, with a maximum power of 7 mW and 632.5 nm wavelength.

Results and discussion

X-ray diffraction (XRD)

Figure 1 presents the X-ray diffraction (XRD) patterns of the TLM samples. All patterns present a halo centered at $27°$, and there is the absence of discrete sharp peaks. This
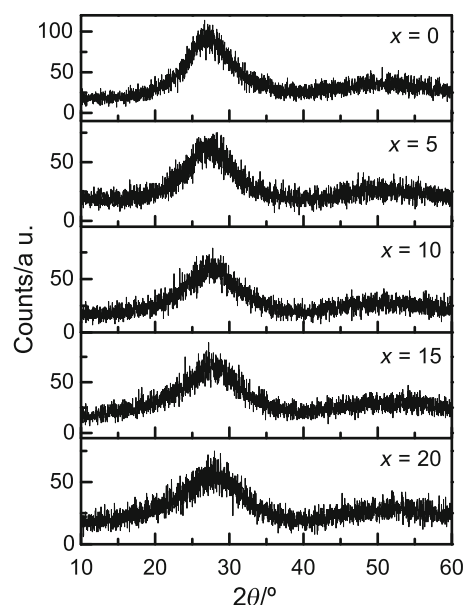

Fig. 1 XRD patterns of TLM samples

reveals the absence of long-range periodicity, indicating the amorphous state of the prepared samples.

Raman spectroscopy

Figure 2a shows the Raman spectra of all samples in the range of 400–1000 cm^{-1}. The notation $_AQ_m^n$ based on refs. [19, 20] was adopted to describe the different structural units presented in Raman results, as shown in Fig. 2b.
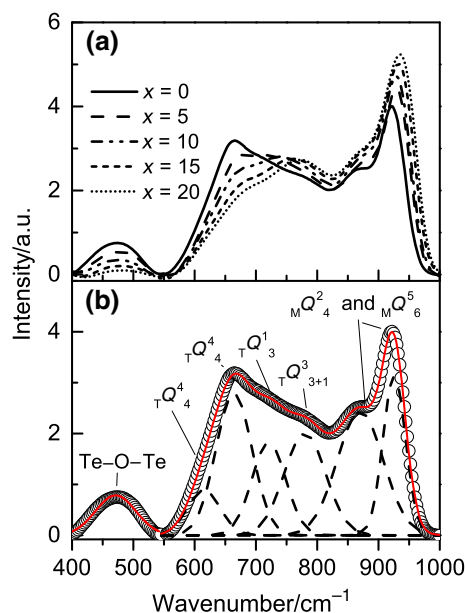

Fig. 2 a Raman spectra of TLM samples. **b** The Gaussian fitting for sample with $x = 0$ mol% indicating the vibration modes centered at 475, 615, 665, 720, 780, 875, and 930 cm^{-1}. (The red line represents Gaussian fitted curve). (Color figure online)

Index A indicates the ion (T for Te or M for Mo), m is the coordination number of structure, n is the number of bridging oxygen (BO) and the $m - n$ difference express number of NBO atoms.

According to the literature, there are seven characteristic bands corresponding to the different structural units present in the TLM glass samples 475, 615, 665, 720, 780, 875 and 930 cm^{-1} [5, 19, 25, 39, 40]. The Raman results were then analyzed by Gaussian fitting, fixing the center of each Gaussian in the positions assigned to each vibration mode (structural unit). A typical result for the sample with $x = 0$ mol% is shown in Fig. 2b. From these fitting, the behavior of the areas for each band (A_{GD}) as a function of x was obtained, and this is presented in Fig. 3.

The band at 475 cm^{-1} is assigned to stretching and bending vibration modes of the Te–O–Te bonds formed by the corner shared from the units $_TQ_4^4$, $_TQ_3^{3+1}$, and $_TQ_1^3$. At 615 cm^{-1} the vibration mode is related to anti-symmetric stretching of continuous network composed of $_TQ_4^4$. The A_{GD} values for these two bands decrease with increasing x. In fact, if the TeO₂ content decreases, which is the primary former oxide for this system, the quantities of the Te–O–Te bonds decrease. In addition, this indicates that adding Li₂O to the glass breaks these bonds [39].

At 665 cm^{-1}, the anti-symmetric stretching of Te$_{ax}$–O$_{eq}$–Te from $_TQ_4^4$ units occurs. Accordingly, this band represents the concentration of this unit. Figure 3 shows the decreasing of A_{GD} with increasing x. This behavior is consistent with the literature [38, 48] in which adding
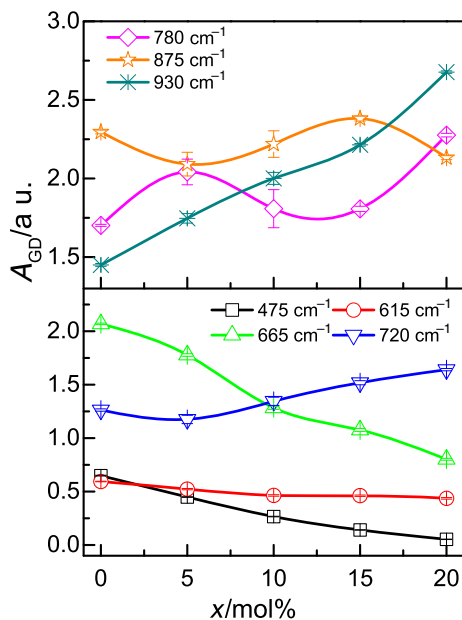
modifier oxides, such as Li₂O, promotes the change of $_TQ_4^4$ to $_TQ_3^{3+1}$ and $_TQ_3^1$.

The stretching vibrations of Te–O$^-$ (NBO) which has Raman mode at 720 cm^{-1} and assigned to $_TQ_3^1$ presents an increase in A_{GD} with x content. This is an additional evidence that addition of Li₂O breaks the Te–O$_{ax}$ bond, forming the $_TQ_3^1$ units.

However, for the stretching vibrations of Te–O$^-$ (NBO) assigned to $_TQ_3^{3+1}$, A_{GD} presented a peculiar behavior: increases from $x = 0$ mol% to $x = 5$ mol%, decreases from $x = 5$ mol% to $x = 10$ mol%, remains constant up to $x = 15$ mol% and then increases again from 15 to 20 mol%. This behavior is opposite to the 875 cm^{-1} which can be attributed to the vibrations of Mo–O–Mo linkages from $_MQ_4^2$ and $_MQ_6^5$ units [26]. In addition, for the vibrations mode assigned to Mo–O–Te linkages at 930 cm^{-1} that bridges the Mo units to the Te ones [41], the A_{GD} increases with x. These behaviors can be attributed to the formation of Mo–O–Te linkages formed from the rearrangement of NBO atoms from $_TQ_3^{3+1}$ units and the breaking of Mo–O–Mo bonds.

Differential scanning calorimetry (DSC)

DSC scans for all compositions are presented in Fig. 4. The T_g is usually taken from the intersection point between the baseline and the tangent line in inflection point at the first change in this baseline. The onset crystallization (T_x) is determined from the second baseline of the above base corresponding to the first exothermic peak at the crystallization temperature (T_c).

Table 1 shows the T_g, T_x and T_c values for all samples. All values obtained for T_g are lower than for TeO₂-pure

Fig. 3 Behavior of the areas of the fitted Gaussian bands (A_{GD}) centered at 475, 615, 665, 720, 780, 875, and 980 cm^{-1}. (the solid lines are only to guide-eyes)
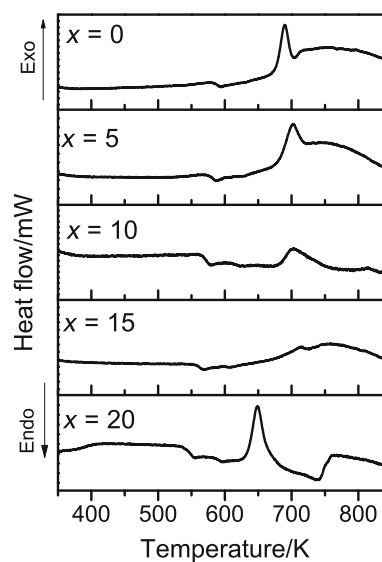

Fig. 4 Heat flow behavior by temperature of vitreous samples

Table 1 Glass transition temperature (T_g), onset crystallization (T_x), Peak at the crystallization temperature (T_c), thermal stability ΔT, Linear Refractive Index n_0 and Polarizability results calculated by Eq. (6).

Samples	Temperatures ($\pm 4\,K$)				ρ_g/g cm^{-3}	M_{W_g}/g mol^{-1}	V_m/cm^3 mol^{-1}	OPD/mol L^{-1}	n_0	$\alpha_{O^{2-}}(n_0)$/Å^3
	T_g	T_x	T_c	ΔT						
TeO$_2$-pure*	598	673	713	75	5.11	159.61	31.29	64.03	2.184	2.659
TLM800020	581	676	689	95	5.27 ± 0.01	156.796	29.75 ± 0.05	73.9 ± 0.1	2.12 ± 0.02	2.18 ± 0.03
TLM700525	572	679	702	107	5.097 ± 0.003	149.611	29.36 ± 0.02	74.95 ± 0.04	2.10 ± 0.01	2.18 ± 0.01
TLM601030	565	682	701	117	4.914 ± 0.001	142.427	28.98 ± 0.01	75.90 ± 0.01	2.07 ± 0.01	2.16 ± 0.01
TLM501535	554	676	713	122	4.721 ± 0.003	135.242	28.64 ± 0.02	76.8 ± 0.3	2.03 ± 0.01	2.13 ± 0.01
TLM402040	537	633	648	96	4.499 ± 0.001	128.058	28.46 ± 0.01	77.29 ± 0.02	1.93 ± 0.02	1.95 ± 0.03

*Values from references [16, 17]

glass, and these values decrease with x content. According to the literature [15, 25, 40], adding Li$_2$O breaks the Te–O$_{ax}$ bonds from $_TQ_4^3$ units, promoting the creation of $_TQ_{3+1}^3$ and $_TQ_3^1$ units. Since the single bond enthalpy of Mo–O is lower than the single bond enthalpy of Te–O, 386 and 428 kJ mol^{-1}, respectively [26], the addition of Li$_2$O also breaks the Mo–O–Mo linkages and promotes the Mo–O–Te bonds. This conclusion is supported by Raman studies which confirm that the peak at 875 cm^{-1} has opposite behavior of 780 cm^{-1} and that the peak at 930 cm^{-1} increases. Thermal stability was estimated by $\Delta T = T_X - T_g$ [1, 6, 14, 16, 29, 42, 46] and is a relevant parameter for technological aspects, by reason of it may represent the degree of disorder in the vitreous structure [45, 46]. Glasses with $\Delta T > 373\,K$ provide a large *working range*, meaning that the glass can be heated above T_g without inducing crystallization [14]. For TLM glasses, all ΔT values are higher than TeO$_2$-pure glassy and also higher than that found for TeO$_2$–MoO$_3$ binary systems [14]. ΔT values increase up to $x = 15$ mol% and then decrease to $x = 20$ mol%. The increase in ΔT indicates that the network connectivity increases, forming the Te–O–Mo bonds. The same behavior was found for TeO$_2$–ZnO–PbO systems where the Te–O–Pb bonds increase the ΔT values, indicating the difficulty for the system to rearrange to the lowest energy configuration (crystal) [35]. However, for $x = 20$ mol% we have the same content of TeO$_2$ and MoO$_3$, so a saturation occurs, and the amount of NBO in Te units available to rearrange with Mo units is not enough, decreasing the glass network connectivity.

According to Aida et al. [1], the resistance against crystallization is improved by the combination of oxides. If the molar ratio between the oxides is different from 1, then the crystallization tendency is pronounced. The concept of ΔT refers to a tendency toward crystallization in the cooling or heating process [37]. Samples with $x = 0$ mol% (TLM800020) and $x = 20$ mol% (TLM402040) present the lowest ΔT, so the crystallization trend is higher than other TLM samples. The best ΔT value was obtained for the sample with $x = 15$ mol% (122 K) (TLM501535). Therefore, these results indicate that the degree of structural disorder in the glass phase of TLM samples makes this system a good candidate for fiber drawing, by means of the resistance to the heating cycles [29, 45].

Density and oxygen packing density (OPD)

To determine the density (ρ_g), the following equation was used:

$$\rho_g = \frac{m_R}{m_R - m_A}\rho_L \tag{1}$$

where m_R is the real mass, m_A is the apparent mass and ρ_L is the density of distilled water, 0.9978 g cm^{-3}. For the molar volume (V_M), the following equation was used:

$$V_M = \frac{M_{W_g}}{\rho_g} \tag{2}$$

where M_{W_g} is the molecular weight of the glass according to a molar percentage (mol):

$$M_{W_g} = (0.8 - 2x)M_{W_{TeO_2}} + xM_{W_{Li_2O}} + (0.2 + x)M_{W_{MoO_3}} \tag{3}$$

where $x = 0.00, 0.05, 0.10, 0.15,$ and 0.20 are molar fractions in mol. In addition, $M_{W_{TeO_2}} = 159.61$ g mol^{-1}, $M_{W_{Li_2O}} = 29.99$ g mol^{-1} and $M_{W_{MoO_3}} = 143.54$ g mol^{-1}. These data also show that it is also possible to calculate the oxygen packing density (OPD) using [4]:

$$OPD = 1000C_O\frac{\rho_g}{M_{W_g}} \tag{4}$$

where $C_O = (0.8 - 2x)q + xs + (0.2 + x)u$ is the number of oxygen atoms in oxide, q, s, and u are the number of oxygen atoms in each cation A, B, and C corresponding to

Te, Li, and Mo atoms, respectively, in the general stoichiometric formula $(0.8 - x)A_pO_q : xB_rO_s : (0.2 + x)C_tO_u$ [8, 9, 11, 12]. Table 1 summarizes the ρ_g, V_m, M_{w_g} and OPD results. The values reported are consistent with previous work for the $x = 0$ mol% (TLM800020) sample [26].

Figure 5 presents the behavior of (OPD), density of the glass (ρ_G), and molar volume (V_m) as a function of x mol%. ρ_g and V_M decrease with the increased x content. In contrast, OPD increases with x mol%. Since molar volume is limited by the space occupied by the structural units of the three oxides forming 1 mol glass. Logically, the molar volume increases: (1) with the number of oxygen atoms; (2) with the proportion and cation radius; (3) when the coordination number increases, and (4) when the field intensity of cations diminishes. Besides, decreasing V_m with increasing OPD with x content indicates structural packing in the glass network, which depends on two main factors: the cation radius and, especially, their field intensity. Therefore, the packing degree is higher for higher cation field intensity and lower cation radius. For TLM, the ionic radius of Mo⁶⁺ and Li⁺ are 0.079 and 0.068 nm, respectively, which are much lower than ionic radius for Te⁴⁺ [4, 24]. In this sense, the formation of Te–O–Mo bonds increases the average cation field intensity with x content, increasing OPD and decreasing V_m. Raman results reinforce the increase in average cation field intensity, since the results of A_{GD} show that the formation of Te–O–Mo bonds (930 cm⁻¹) is much higher than the transformation of TeO₄-units (615–665 cm⁻¹) to TeO₃-units (720 cm⁻¹).
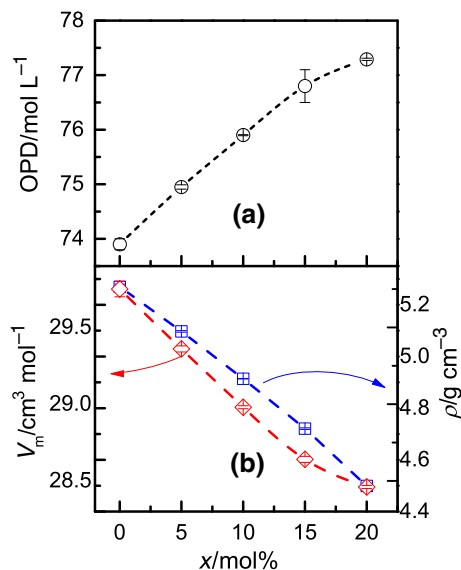
Linear refractive index and electronic polarizability

The refractive index is one of the important properties in optical glass and it is closely related to the electronic polarization of the ions and the local field inside the glass, especially in connection with the theory of electronic structure of glasses that is directly related to the performance of optical fibers. Thus, it is necessary to understand the effect of introducing network ions into tellurite-rich glasses by measuring their refractive index [28]. The values obtained for n_0 are presented in Table 1. All values are lower than for TeO₂-pure glass.

Figure 6 shows the behavior of n_0 values with x content and shows a slightly decrease in n_0 values up to $x = 15$ mol%. With $x = 20$ mol%, the n_0 value decreases abruptly from ~ 2 to 1.93. because the conversion from $_TQ_4^4$ to $_TQ_{3+1}^3$ and $_TQ_3^1$ units.

Ab initio quantum chemical calculations performed by others indicate that the polarizability of the $_TQ_3^1$ subunit is substantially less than the $_TQ_4^4$ [18]. Therefore, the conversion of $_TQ_4^4$ to $_TQ_3^1$ results in a decrease in the polarizability of the fundamental constituents of the glass network [24]. Hence, the decrease in n_0 correspond to a lower polarizability of the glassy network [30]. To confirm the previous statement, the electronic polarizabilities of TLM samples were determined.

The general stoichiometric relation $xA_pO_q : yB_rO_s : zC_tO_u$ was used, where p, r, and t are cation numbers and q, s, and u are oxygen numbers. Using the Lorentz–Lorenz equation, the average electronic polarizability $\alpha_{O^{2-}}(n_0)$ for ternary glasses can be determined by equation proposed by Dimitrov and Komatsu [8]:

$$\alpha_{O^{2-}}(n_0) = \left[\left(\frac{V_m}{2.52} \right) \frac{(n_0^2 - 1)}{(n_0^2 + 2)} - \sum_{i=0}^{3} \alpha_i \right] \frac{1}{N_{O^{2-}}} \tag{5}$$

where V_m is the molecular volume, n_0 is the refractive

Fig. 5 Behavior of **a** Oxygen Packing Density OPD and Glassy transition T_g and **b** Density of the glass ρ_G and Molar Volume V_m as a function of x mol% (Dashed lines are guide-eyes)
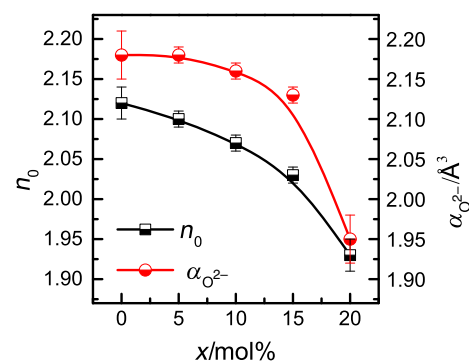

Fig. 6 n_0 and $\alpha_{O^{2-}}(n_0)$ versus x content of samples(Solid lines are guide-eyes)

index, $N_{O^{2-}} = xq + us + zu$, and the sum of the molar polarizabilities of the cations is given by:

$$\sum_{i=A,B,C}^{3} \alpha_i = (1 - x_{Li_2O} - y_{MoO_3})p\alpha_A + x_{Li_2O}r\alpha_B + y_{MoO_3}t\alpha_C$$

(6)

with $\alpha_A = \alpha_{TeO_2} = 1.595\,\text{Å}^3$, $\alpha_B = \alpha_{Li_2O} = 0.024\,\text{Å}^3$ and $\alpha_C = \alpha_{MoO_3} = 0.169\,\text{Å}^3$ [12]. The calculated electronic polarizabilities values for the TLM samples are given in Table 1. Figure 6 presents the values of $\alpha_{O^{2-}}(n_0)$ with x content. It can be observed that the values of $\alpha_{O^{2-}}(n_0)$ decrease with increased x content. Since $_TQ_4^4$ units possess high field intensity with very high polarizability (1.595 Å), a glass containing only $_TQ_4^4$ units presents high values of oxide ion polarizability [1]. However, by adding Li_2O and MoO_3 to the glass, there is a transformation to $_TQ_{3+1}^3$ and $_TQ_3^1$ units and the formation of Te–O–Mo bonds. Considering that the electronic polarizabilities of $_TQ_4^4$ and $_TQ_{3+1}^3$ are much higher than the polarizabilities of the $_TQ_3^1$ units, the behavior of $\alpha_{O^{2-}}(n_0)$ with x content can be attributed to the increase in Te–O–Mo bonds, since the Te–O bonds in the structure of tellurite glasses have a significant effect on electronic polarizability.

This variation in polarizability has a direct impact on refractive index behavior, since the refractive index of tellurite glasses is accounted to the high polarizability of an electronic lone pair in one of the sp^3d hybridized orbitals of the $_TQ_4^4$ units and electron delocalization effects. The addition of other oxides in TeO_2 network can cleaves a Te–O bond in the $_TQ_4^4$ creating a $_TQ_3^1$ structure, as mentioned before, changing the polarizability. Indeed, the refractive index can also be dependent of the polarizability of the additive oxide, in this case, the polarizability of MoO_3 is higher than TeO_2. However the cleave occurring in Te–O–Mo bonds can change the electron delocatization effects in Te units, which could explains the decrease in refractive index.

Conclusions

Structural and thermal properties o $(80 - 2x)TeO_2 - xLi_2O - (20 + x)MoO_3$ glasses were studied by using Raman spectroscopy, differential scanning calorimetry, density and Brewster angle technique. Our results show that adding Li_2O influenced the breaking of Te–O–Te bonds, which connect the Te units, but also on the Mo–O–Mo bonds. Consequently, the formation of Te–O–Mo linkages increases the thermal stability up to $x = 15\,mol\%$ and then decreases to $x = 20\,mol\%$. This decrease has been attributed to a saturation on the NBO content available to

rearrange with Mo units. Another consequence of the Te–O–Mo bond formation is the increase in OPD which increases the average cation field intensity on the glassy system. In addition, the refractive index and electronic polarizabilty values decrease due to the change in the electron delocatization effects in Te units. These insights regarding the TLM system showed that the adding Li_2O in TeO_2–MoO_3 system can enhance the thermal stability and change the electronic polarizability, making the TLM system a potential material for technological applications.

References

1. Aida K, Komatsu T, Dimitrov V. Thermal stability, electronic polarisability and optical basicity of ternary tellurite glasses. Phys Chem Glasses. 2001;42(2):103–11.
2. Brady GW. Structure of tellurium oxide glass. J Chem Phys. 1957;27(1):300–3.
3. Capanema W, Yukimitu K, Moraes JCS, Santos FA, Figueiredo MS, Sidel SM, Reynoso VCS, Sakai OA, Medina AN. The structure and optical dispersion of the refractive index of tellurite glass. Opt Mater. 2011;33(11):1569–72.
4. Çelikbilek M, Erçin Ersundu A, Aydin S. Glass formation and characterization studies in the TeO_2-WO_3-Na_2O system. J Am Ceram Soc. 2013;96(5):1470–6.
5. Chowdari BVR, Tan KL, Ling F. Synthesis and characterization of $xCu_2o\cdot\cdot yTeO_2\cdot\cdot(1\text{-}x\text{-}y)MoO_3$ glass system. Solid State Ion. 1998;113:711–21.
6. Dietzel A. Glass structure and glass properties. Glasstech. 1968;22:41.
7. Dimitriev Y, Dimitrov V, Arnaudov M. Ir spectra and structures of tellurite glasses. J Mater Sci. 1983;18(5):1353–8.
8. Dimitrov V, Komatsu T. Electronic polarizability, optical basicity and non-linear optical properties of oxide glasses. J Non Cryst Solids. 1999;249(2):160–79.
9. Dimitrov V, Komatsu T. An interpretation of optical properties of oxides and oxide glasses in terms of the electronic ion polarizability and average single bond strength. J Univ Chem Technol Metall. 2010;45(3):219–50.
10. Dimitrov V, Komatsu T. Optical basicity and chemical bonding of ternary tellurite glasses. Phys Chem Glasses Eur J Glass Sci Technol Part B. 2014;55(1):13–7.
11. Dimitrov V, Komatsu T. Polarizability, basicity and chemical bonding of single and multicomponent oxide glasses. J Chem Technol Metall. 2015;50(4):387–96.
12. Dimitrov V, Sakka S. Electronic oxide polarizability and optical basicity of simple oxides. I. J Appl Phys. 1996;79(3):1736–40.
13. El-Mallawany R. The optical properties of tellurite glasses. J Appl Phys. 1992;72(5):1774–7.
14. El-Mallawany R. Devitrification and vitrification of tellurite glasses. J Mater Sci Mater Electron. 1995;6(1):1–3.
15. El-Mallawany R. Tellurite glasses: Part 2. Anelastic, phase separation, debye temperature and thermal properties. Mater Chem Phys. 1999;60(2):103–31.
16. El-Mallawany RA. Tellurite glasses handbook: physical properties and data. Boca Raton: CRC press; 2011.
17. Elkhoshkhany N, El-Mallawany R, Syala E. Mechanical and thermal properties of TeO_2–Bi_2O_3–V_2O_5–Na_2O–TiO_2 glass system. Ceram Int. 2016;42(16):19,218–24.

18. Fargin E, Berthereau A, Cardinal T, Le Flem G, Ducasse L, Canioni L, Segonds P, Sarger L, Ducasse A. Optical non-linearity in oxide glasses. J Non Cryst Solids. 1996;203:96–101.

19. Gomes JL Jr, Piazzetta RLS, Gonçalves A, Somer A, da Cruz GK, Serbena FC, Novatski A. Correlation between nonbridging oxygens and the thermal and optical properties of the TeO$_2$-Li$_2$O-MoO$_3$ glassy system. J Mater Res. 2015;30(16):2417–24.

20. Gulenko A, Masson O, Berghout A, Hamani D, Thomas P. Atomistic simulations of TeO$_2$-based glasses: interatomic potentials and molecular dynamics. Phys Chem Chem Phys. 2014;16(27):14,150–60.

21. Hajer S, Halimah M, Azmi Z, Azlan M. Optical properties of zinc–borotellurite doped samarium. Chalcogenide Lett. 2014;11(11):553–66.

22. Halimah M, Daud W, Sidek H, Zaidan A, Zainal A. Optical properties of ternary tellurite glasses. Mater Sci Pol. 2010;28(1):173–80.

23. Jauhariyah MN, Setyarsih W, Yantidewi M, Marzuki A, et al. Refractive index measurement of tellurite glasses by using Brewster angle method. In: Sensors, instrumentation, measurement and metrology (ISSIMM), international seminar on. IEEE; 2016. pp. 71–4.

24. Jose R, Arai Y, Ohishi Y. Optical properties of MoO$_3$ containing tellurite glasses. Appl Phys Lett. 2008;93(16):161–901.

25. Kalampounias AG, Boghosian S. Distribution of tellurite polymorphs in the xM$_2$O-(1- x)TeO$_2$ (M= Li, Na, K, Cs, and Rb) binary glasses using Raman spectroscopy. Vib Spectrosc. 2012;59:18–22.

26. Kaur A, Khanna A, González F, Pesquera C, Chen B. Structural, optical, dielectric and thermal properties of molybdenum telluride and borotellurite glasses. J Non Cryst Solids. 2016;444:1–10.

27. Kim SH, Yoko T, Sakka S. Linear and nonlinear optical properties of Teo$_2$ glass. J Am Ceram Soc. 1993;76(10):2486–90.

28. Lakshminarayana G, Kaky KM, Baki S, Lira A, Nayar P, Kityk I, Mahdi M. Physical, structural, thermal, and optical spectroscopy studies of TeO$_2$-B$_2$O$_3$-MoO$_3$-ZnO-R$_2$O (R= Li, Na, and K/MO (M= Mg, Ca, and Pb) glasses. J Alloys Compd. 2017;690:799–816.

29. Manikandan N, Ryasnyanskiy A, Toulouse J. Thermal and optical properties of TeO$_2$-ZnO-BaO glasses. J Non Cryst Solids. 2012;358(5):947–51.

30. Manning S, Ebendorff-Heidepriem H, Monro TM. Ternary tellurite glasses for the fabrication of nonlinear optical fibres. Opt Mater Express. 2012;2(2):140–52.

31. Mekki A, Khattak G, Wenger L. Structural and magnetic properties of MoO$_3$-TeO$_2$ glasses. J Non Cryst Solids. 2005;351(30–32):2493–500.

32. Moraes JCS, Nardi J, Sidel S, Mantovani B, Yukimitu K, Reynoso V, Malmonge L, Ghofraniha N, Ruocco G, Andrade L, et al. Relation among optical, thermal and thermo-optical properties and niobium concentration in tellurite glasses. J Non Cryst Solids. 2010;356(41):2146–50.

33. Nasu H, Matsushita O, Kamiya K, Kobayashi H, Kubodera K. Third harmonic generation from Li$_2$O-TiO$_2$-TeO$_2$ glasses. J Non Cryst Solids. 1990;124(2–3):275–7.

34. Pal M, Hirota K, Tsujigami Y, Sakata H. Structural and electrical properties of MoO$_3$-TeO$_2$ glasses. J Phys D Appl Phys. 2001;34(4):459.

35. Ramamoorthy RK, Bhatnagar AK. Effect of ZnO and PbO/ZnO on structural and thermal properties of tellurite glasses. J Alloys Compd. 2015;623:49–54.

36. Reben M, Grelowska I, Kosmal M, Szumera M, et al. Influence of modifiers on the thermal characteristic of glasses of the Teo$_2$-P$_2$O$_5$-ZnO-PbF$_2$ system. J Therm Anal Calorim. 2016;125(3):1279–86.

37. Saad M, Poulain M. Glass forming ability criterion. In: Mat. Sci. Forum, 1987; vol. 19, pp. 11–18. Trans Tech Publ

38. Sakida S, Hayakawa S, Yoko T. Part 2. 125 Te NMR study of M$_2$O-TeO$_2$ (M= Li, Na, K, Rb and Cs) glasses. J Non Cryst Solids. 1999;243(1):13–25.

39. Sekiya T, Mochida N, Ogawa S. Structural study of MoO$_3$-TeO$_2$ glasses. J Non Cryst Solids. 1995;185(1–2):135–44.

40. Sekiya T, Mochida N, Ohtsuka A, Tonokawa M. Raman spectra of Mo$_{1/2}$-TeO$_2$ (m= Li, Na, K, Rb, Cs and Tl) glasses. J Non Cryst Solids. 1992;144:128–44.

41. Sokolov V, Plotnichenko V, Koltashev V, Grishin I. On the structure of molybdate-tellurite glasses. J Non Cryst Solids. 2009;355(4–5):239–51.

42. Souri D. Physical and thermal characterization and glass stability criteria of amorphous silver-vanadate-tellurate system at different heating rates: Inducing critical Ag$_2$O/V$_2$O$_5$ ratio. J Non Cryst Solids. 2017;475:136–43.

43. Souri D, Elahi M. Effect of high electric field on the dc conduction of TeO$_2$-V$_2$O$_5$-MoO$_3$ amorphous bulk material. Czechoslov J Phys. 2006;56(4):419–25.

44. Souri D, Honarvar F, Tahan ZE. Characterization of semiconducting mixed electronic-ionic TeO$_2$V$_2$O$_5$Ag$_2$O glasses by employing ultrasonic measurements and vicker's microhardness. J Alloys Compd. 2017;699:601–10.

45. Souri D, Mohammadi M, Zaliani H. Effect of antimony on the optical and physical properties of Sb-V$_2$O$_5$-TeO$_2$ glasses. Electron Mater Lett. 2014;10(6):1103–8.

46. Souri D, Shahmoradi Y. Calorimetric analysis of non-crystalline TeO$_2$-V$_2$O5-Sb$_2$O$_3$. J Therm Anal Calorim. 2017;129(1):601–7.

47. Souri D, Shomalian K. Band gap determination by absorption spectrum fitting method (asf) and structural properties of different compositions of (60-x)V$_2$o$_5$-40TeO$_2$-xSb$_2$o$_3$ glasses. J Non Cryst Solids. 2009;355(31–33):1597–601.

48. Tanaka K, Yoko T, Yamada H, Kamiya K. Structure and ionic conductivity of LiCl- Li$_2$O-TeO$_2$ glasses. J Non Cryst Solids. 1988;103(2–3):250–6.

49. Tikhonova EL, Lyakaev DV, Grishin IA, Kotkova AM, Markin AV. Thermodynamic properties of (TeO$_2$)$_n$ (MoO$_3$)$_{1-n}$ glasses. Inorg Mater. 2017;53(11):1201–8.

50. Yukimitu K, Oliveira R, Araujo E, Moraes JCS, Avanci L. DSC studies on crystallization mechanisms of tellurite glasses. Thermochim Acta. 2005;426(1–2):157–61.